

## Modeling High-Burnup BWR Fuel Behavior During RIA

Wenfeng Liu and Mujid S. Kazimi\*

*Center for Advanced Nuclear Energy Systems,  
Department of Nuclear Science and Engineering,  
Massachusetts Institute of Technology,  
77 Massachusetts Avenue, Cambridge, MA 02139*

**Abstract** - *This paper describes models for fission gas release (FGR) and swelling and clad brittle failure due to pellet cladding mechanical interaction (PCMI) introduced in the FRAPTRAN code and their applications to BWR test rods during reactivity initiated accident (RIA) conditions.*

*The FGR model takes into account the contribution from both the fission gas in the rim and intergranular bubbles in the inner fuel. It assumes a burst release occurs once the pellet clad gap is sufficiently large for the gas to flow into the plenum. The fission gas induced swelling is modelled as the relaxation of over-pressurized pores in the rim by a dislocation loop punching mechanism as well as by gas expansion after grain boundary separation. The application of the model to the BWR fuel rods reveals that the relatively larger gap sizes would enable fission gas release in the early phase of the transient. Thus less fission gas remains in the pellet to contribute to cladding deformation.*

*PCMI failure is modelled based on fracture mechanics. The focus is on capturing the underlying physical mechanisms including: a) A flaw size model considering the oxide layer and the  $\delta$ -phase hydride, b) A fracture toughness model encompassing both hydrided and irradiated cladding property, and c) A fracture failure strain criterion to predict PCMI failure. The new model is capable of partitioning the failed and non-failed rods capturing the effects of different burnup levels and fuel enthalpy deposition. Furthermore, the model indicates that the enthalpy deposition at failure is somehow controlled by the crack propagation in the remaining ductile ligament. This model also reveals that for a wider power pulse, a higher threshold of the enthalpy is required for PCMI failure.*

### I Introduction

As economic advantages stimulate increasing discharge burnup of LWR fuels, safety concerns have been raised about the fuel performance particularly during the operational and postulated transient conditions. Several test facilities at NSRR<sup>1)</sup>, CABRI<sup>2)</sup> and IGR/BIGR<sup>3)</sup> have provided valuable information concerning the behaviour of high burnup fuel during RIA conditions. This enables improvement in modeling the transient fuel performance based on the rich information from

these experiments. A general understanding has been reached from the experiments and fuel models on the role of pellet thermal expansion in the PCMI failure, effects of the hydride on the cladding integrity and post-DNB cladding temperature excursions<sup>4)</sup>. However, it's still difficult to extrapolate these results to realistic LWR conditions. Therefore, our efforts are directed towards developing mechanistic models for fission gas behaviour, PCMI failure and heat transfer at DNB conditions in the transient fuel performance code and applying these models to analyze the behaviour of high burnup fuel rods in LWRs.

---

\*Tel: +1 617 253 4206, Fax: +1 617 258 8863,  
Email: kazimi@mit.edu

In this paper a progress report is given on modeling fission gas release, fission gas induced swelling, and clad brittle failure due to PCMI in the MIT version of the FRAPTRAN code and their applications to the FK test series at the NSRR.

The FGR and fission gas induced swelling models are described in a previous publication<sup>5)</sup>, this paper will focus on the application of the models to the BWR test rods. As a first attempt to model PCMI failure using fracture mechanics, we focus on capturing the underlying physical mechanisms including: a) A flaw size model considering the oxide layer and the  $\delta$  phase hydride, b) A fracture toughness model encompassing both hydrided and irradiated cladding property, and c) A fracture failure strain criterion to predict PCMI failure.

Input cases from FK1 to FK9 for FRAPTRAN are prepared based on the data extracted from literature.<sup>6-9)</sup> Parameters describing the test conditions and experiment data used to compare code calculation results are listed in Table 1.

## II Modeling Fission Gas Behavior

The FGR model accounts for the fission gas stored in the fuel peripheral pores as well as the inter-granular bubbles in the grain boundary of the inner fuel regions. The amount of fission gas in the rim-zone in [%w] is given as the xenon depletion<sup>10)</sup>.

$$Xe_c = \dot{c}BU - \dot{c} \left\{ \frac{1}{a} + \left( BU_0 - \frac{1}{a} \right) e^{[-a(BU-BU_0)]} \right\} \quad (1)$$

where  $\dot{c}$  is the xenon production rate in [%w / BU],  $BU_0$  is a threshold burnup for the xenon depletion measured in [GWd / tU],  $BU$  is the local burnup and  $a$  is a constant measured in the reciprocal of BU units related to the xenon equilibrium concentration. The quantity of fission gas on the grain boundaries and in the grains during steady state operation simulated by FRAPCON to initialize FRAPTRAN is still uncertain<sup>11)</sup>. Therefore, the fission gas inventory in the intergranular bubbles is estimated by the

saturation assumption at End-Of-Life (EOL). The gas concentration  $G_{BS}$  in [atoms/m<sup>3</sup>] is given by

$$G_{BS}(r) = \left[ \frac{2r_b f(\theta) f_c}{r_{gr} k_B T_0(r) \sin^2(\theta)} \right] \left[ p_{H0} + \frac{2\gamma}{r_b} \right] \quad (2)$$

where  $\theta$  is semi-dihedral angle,  $r_{gr}$  is the grain radius in [m],  $r_b$  is the intergranular bubble radius in [m],  $T_0$  [K] is temperature at EOL,  $p_{H0}$  is hydrostatic pressure,  $f_c$  is the fractional gas coverage of grain boundary at saturation,  $k_B$  is the Boltzmann constant and  $f(\theta) = 1 - 3\cos\theta/2 + \cos^3\theta/2$ .

The burst release model assumes that open porosity connects the gas plenum to the percolated fuel as the grain boundary is cracked by the following criterion<sup>12)</sup>.

$$p > p_s + \frac{p_H}{f} + \left( \frac{1-f}{f} \right) \sigma_r \quad (3)$$

where  $f$  is the grain surface gas coverage fraction,  $p_s$  [Pa] is the surface tension pressure and  $\sigma_r$  is the fracture stress of grain boundary in [Pa]. An instantaneous gas emission is assumed once the clad-fuel deformation creates an open gap sufficiently large for the gas to flow into the plenum.

The swelling is modeled as the relaxation of over-pressurized pores in the rim by a dislocation loop punching mechanism as well as by gas expansion after grain boundary separation. The porosity fitting in the rim region is given to calculate the pressure of the pores in the rim region<sup>5)</sup>.

Several modifications of the models in our earlier work<sup>5)</sup> have been made. The burnup profile produced by a neutronic code<sup>8)</sup> is substituted into Eq. (1) to compute the fission gas inventory in the rim region. Recognizing that fuel recrystallization and xenon depletion doesn't take place simultaneously in the peripheral region of the pellet<sup>13)</sup>, this approach would be more appropriate to calculate xenon depletion than using a rim size model. An incubation threshold burnup model<sup>14)</sup> as a function of operating temperature predicting the onset of saturation of intergranular fission gas is introduced in Eq. (4).

$$B_I = \frac{B_1}{\exp(-T_{02}/T) + (T - T_1)/T_2} + B_2 \quad (4)$$

where  $B_I$  is the incubation burnup at temperature  $T$  (K) and  $B_1 = 0.0012$  GWd/tM,  $B_2 = 2.5$  GWd/tM,  $T_1 = 603$  K, and  $T_2 = 1.59 \times 10^7$  K are model parameters. Base irradiation is simulated by the FRAPCON code to provide the operating temperature in the last cycle. The temperature at each radial node averaged in the last cycle is plugged into Eq. (4) to calculate the incubation burnup as a function of pellet radius. This incubation burnup is compared with the burnup at each radial node to determine whether the saturation has been achieved.

## 1 Fission Gas Release

The results for fission gas release are shown in Figure 1. The fission gas release prediction shows good agreement for FK4 and FK6 with relatively higher burnup and higher enthalpy deposit. The other cases show somewhat over-prediction. Applying the incubation threshold-burnup model reveals that there is almost no saturation in the inner fuel for cases FK1-FK3. This is also evidenced by the low fission gas release fraction with relatively lower linear heat rate during the base irradiation. Since the incubation threshold burnup model excludes the fission gas from the unsaturated grain boundary during a transient, it can be seen as a lower bound of the fission gas prediction. Even in this lower bound calculation, FK2, FK5 and FK8 still show over-prediction. Since cases FK2, FK5 and FK8 have relatively lower enthalpy deposition and wider power pulse, less driving force would be expected for the fission gas release. Fuel fragmentation<sup>5)</sup> is considered as the main reason for formation of gas release path during the transient, for which the resistance force is taken into account by the fracture stress of the grain boundary. It turns out that for FK2, FK5 and FK8, the fuel fragmentation rule Eq. (3) doesn't work well without considering the details in the formation of fission gas release path. Thus developing a detailed mechanism for fission gas release after grain

boundary cracking is still necessary. Therefore the current fission gas release model gives conservative predictions for the fission gas effects.

Figure 2 and Figure 3 give the kinetics of the current fission gas release model. There is no fission gas release model in FRAPTRAN1.2, thus the pressure predicted by the FRAPTRAN1.2 can be seen as the pressure due to filling gas, which reaches a maximum value of around 1MPa, obviously lower than the experimental value. This indicates that the rapid pressure increase above 1.5MPa in the experiment in the early phase is due partly to the fission gas release. For case FK4, the code FRATRAN1.2\_MIT gives a good prediction of FGR that matches the experiment, thus the plenum pressure at the rod cooling phase shows the same trend. But in the early phase of RIA, the plenum pressure predicted by FRAPTRAN1.2\_MIT is higher than the experimental value. As seen from Figure 3, the model also gives two stages of fission gas release once the fuel fragmentation rule and open gap condition are satisfied. Code calculation gives that the first fission gas release amount around 8% comes from the rim region of the fuel. This is mainly due to the radial power peaking at the rim of high burnup fuel giving high initial temperature in the rim region. Right after the power pulse, additional fission gas from the center fuel region is released. The pressure increase due to the rim gas predicted by the fission gas release model is around 2MPa. This agrees with the fast release above 1.5MPa in the early phase of the experiment. It implies that some fission gas released slower later on. Most likely, it's due to the frictional resistance as the gas flows from in the percolated fuel.

## 2 Fission Gas Induced Deformation

Since a rigid pellet and thermal expansion model is featured in FRAPTRAN, this tends to over-predict the hoop deformation of the cladding. FRAPTRAN1.2 gives generally higher predictions of the permanent hoop strain, especially for the case

FK4 which has a relatively high enthalpy deposit and small gap size. As the fission gas induced swelling model is introduced, no appreciable change of the cladding deformation can be seen except for The cladding deformation induced by fission gas can be characterized into two scenarios: i) open gap ii) close gap. The latter could be more effective as the fission gas still remains in the pellet at high temperature. Application of the FGR model reveals that for most cases, the relatively larger gap sizes in the BWR fuel rods at cold zero power (CZP) conditions would provide sufficient free volume during the fuel fragmentation. This enables fission gas release in the early phase of the transient, thus less fission gas remains in the fuel to contribute to the cladding deformation. Also the conservative model for thermal expansion could partly counter the effects of the fission gas induced deformation because the constraint by the cladding is taken into account in the fission gas induced deformation model but it's not considered in the thermal expansion model.

Note that for FK6, PCMI failure occurs, and a very small residual hoop strain consistent with the experimental result is predicted by the PCMI failure model in FRAPTRAN1.2\_MIT. In comparison with the prediction by FRAPTRAN 1.2 without PCMI failure, it's unlikely that fission gas induced swelling could contribute to the PCMI loading.

### III Modeling of PCMI failure

It is well recognized that brittle failure of the test rods due to PCMI is the major failure mechanism during the early phase of RIA. This PCMI failure is observed for the BWR rods at burnup above 61 MWd/kg.<sup>7,15)</sup> Post irradiation examination of the cladding indicates that the hydrogen absorbed play an important role in embrittlement of the cladding, with the formation of the  $\delta$  phase hydride. Therefore this failure process is referred to as hydride assisted process. Separate effects of the hydride on the burst stress<sup>16-17)</sup> shows that cladding with hydride rim accumulated near the outer surface is susceptible to

case FK3, for which an increase of hoop deformation could be due to an over prediction of fission gas inventory at the grain boundary.

failure with respect to the cladding with a uniform hydride distribution. This implies that the denser distribution of the hydride near the outer surface of the cladding is also an important parameter affecting the PCMI failure. The radial oriented hydride platelet observed in the recrystallized Zr-2 cladding at high burnup<sup>7)</sup> also decrease the margin to failure because the loading type during RIA could have larger axial /hoop stress ratio than burst test conditions.

Given these observations, we assume the physical process during PCMI loading is that cracks firstly initiated near the outer surface of the cladding with relatively dense hydride at a low stress. The cracking of the zirconia layer in the outermost region of the cladding is also assumed to be pre-existent due to its brittle nature. The cracks initiated at the oxide layer and dense hydride rim propagate axially as well as through the thickness of the cladding depending on the initial crack sizes and the fracture toughness of the cladding.

A method based on fracture mechanics has the advantage to capture this phenomenon. Recognizing that some difficulties exist in the accurate presentation of the hydride distribution and orientation, which is largely controlled by the operating history, simplification is made in the model presented which includes a) the prediction of the flaw size b) fracture toughness model and c) fracture strain at which failure occurs. In this model we neglect the axial crack propagation and assume that a single crack perpendicular to the hoop direction, with a depth controlled by the oxide layer and hydride rim thickness is pre-existing. Once the deformation is large enough to reach the fracture strain, the crack propagates instantly through the wall thickness leading to failure of the cladding.

## 1 Fracture Toughness Model

In general, the temperature, hydrogen content, hydride orientation, fast fluence could modify the fracture toughness of the cladding at high burnup. However no single experiment could cover such a wide range of parameters. Axially notched ring Zr-2 specimen cut from the cladding tube<sup>18-19)</sup> and  $\beta$  treated Zr-4 compact tension specimens tests<sup>20)</sup> are selected for fitting the fracture toughness model. The data and fracture toughness model is shown in Figure 5. PL refers to pin loading. CT refers to compact tension.

As seen from Figure 5, the fracture toughness for both the unirradiated and irradiated hydride specimens decreases as hydrogen content increases at room temperature. In comparison to the specimens at room temperature, the fracture toughness increases at 573K for both the irradiated and unirradiated specimens. This increase could be best characterized by the brittle to ductile transition. At 573K, no major difference for the fracture toughness of the irradiated is shown for hydrogen content up to 500ppm. For unirradiated sample this cut-off hydrogen content could be even higher. These data are consistent with the conclusion that radiation damage controls ductility for hydrogen content up to 800 ppm at reactor operating temperature<sup>21)</sup>, although the cut-off hydrogen content is higher. Therefore two curves representing the fracture toughness at both room temperature and reactor operating temperature are fitted. The ductile to brittle transition temperature (DBTT) is introduced to differentiate the two curves.

T>DBTT

$$K_{IC} = \begin{cases} 116.9 - 0.00782C_H & 0 \leq C_H < 411.3 \text{ ppm} \\ 855.3 \exp(-0.005C_H) & 411.3 \text{ ppm} \leq C_H < 806.1 \text{ ppm} \\ 19.38 - 0.00257C_H & 806.1 \text{ ppm} \leq C_H \end{cases}$$

T<DBTT

$$K_{IC} = \begin{cases} 42.64 \exp(-0.001619C_H) & 0 \leq C_H < 532.4 \text{ ppm} \\ 19.38 - 0.00257C_H & 532.4 \text{ ppm} \leq C_H \end{cases}$$

DBTT is also a function of strain rate,<sup>22)</sup> for highly irradiated cladding, DBTT is 473K at a strain rate of

0.015, and 573K at a strain rate of  $5 \text{ s}^{-1}$ . Given that the high strain rate measured during RIA is in an order of tens %/s<sup>13)</sup>, the DBTT is set as 500K during the PCMI loading phase.

The fracture toughness is modeled by the hydrogen content and temperature being below or above DBTT. The non-uniformity of fracture toughness due to preferential accumulation of hydride at the outer region of the cladding is not modeled. Instead, we consider it in the flaw size model to account for the non-uniform distribution of hydrides.

## 2 Flaw Size

The dense hydride formed at the outer cladding surface prior to the RIA transient is primarily driven by the temperature gradient across the cladding. Considering the low fracture stress of the hydride, the dense hydride rim is assumed to have pre-existing cracks. This hydride rim together with the oxide layer forms the initial flaw in the fracture model.

To predict the flaw size, the hydride rim formation during the steady state is solved as follows. Neglecting the diffusion of  $\delta$ -phase hydride, equations for hydrogen precipitation and diffusion are given as follows<sup>23)</sup>:

$$\frac{\partial C}{\partial t} + \nabla(v_\alpha \bar{J}_\alpha) = 0 \quad (5)$$

$$\bar{J}_\alpha = -D_\alpha (\nabla C_\alpha + \frac{Q_\alpha C_\alpha}{RT^2} \nabla T) \quad (6)$$

$$C = v_\alpha C_\alpha + v_\delta C_\delta \quad (7)$$

$$C_\alpha(r, t) = \min\{C(r, t), TSS\} \quad (8)$$

$$D_\alpha = D_0 \exp(-Q/RT) \quad (9)$$

where subscript  $\alpha$  and  $\delta$  denote  $\alpha$ -phase and  $\delta$ -phase respectively.

$v_\alpha$  is volumetric fraction of  $\alpha$ -phase.

$v_\delta$  is volumetric fraction of  $\delta$ -phase.

$J_\alpha$  is hydrogen flux in  $\alpha$ -phase in [ppm m/s].

$C$  is the total concentration of hydrogen in [ppm].

$C_\alpha$  is the concentration of hydrogen in  $\alpha$ -phase in [ppm].

$C_\delta = 16000$  ppm is the concentration of hydrogen in  $\delta$ -phase.

$R = 8.314$  J/mol-K is the ideal gas constant

$D_0 = 0.27$  mm<sup>2</sup>/s<sup>24</sup>) is diffusion factor

$Q = 35196 \pm 1680$  J/mol<sup>24</sup>) is activation energy for diffusion

$Q_\alpha$  is heat of transport = 20930 J/mol<sup>21</sup>)

$$TSS = K \exp(-H / RT) \quad (10)$$

$TSS$  is the terminal solid solubility of hydrogen in  $\alpha$  phase in [ppm]

$H = 39060$  J/mol<sup>25</sup>) is heat of mixing.

$K = 1.99 \times 10^5$  ppm<sup>25</sup>) is constant for terminal solid solubility.

Assume: a) Diffusion of hydride can be neglected. b) Precipitation and dissolution occurs instantly. c) Steady state at EOL. Following above assumptions, hydrogen diffusion would be driven under the temperature gradient to the cold surface, where a continuum hydride rim is formed. Since diffusion of  $\delta$ -phase hydride is neglected, in the two phase region, hydrogen flux from  $\alpha$ -phase must be zero at steady state, at the same time, the hydrogen concentration of  $\alpha$ -phase must satisfy the terminal solid solubility. Thus the two phase region can only exist at the interface separating  $\delta$ -phase hydride rim from the  $\alpha$ -phase solid solution.

$$V_H = C_\delta t_H + \int_{R_i}^{R_o - t_H} 2\pi r C_\alpha(r) dr \quad (11)$$

$$C_\alpha(R_o - t_H) = TSS(T(R_o - t_H)) \quad (12)$$

$$\frac{dC_\alpha}{dr} + \frac{Q_\alpha C_\alpha}{RT^2} \frac{dT}{dr} = 0 \quad (13)$$

where  $V_H$  is total hydrogen pickup from the water side corrosion.  $t_H$  is the thickness of continuous hydride rim. Given the cladding outside temperature and the temperature gradient (determined by the average linear heat generation rate during the steady state), the temperature distribution is known. Plugging into the above equations, the thickness of the continuous solid hydride rim can be solved. The practical effective flaw size in [m] is set as:

$$a = t_o + \lambda t_H \quad (14)$$

where  $t_o$  is the thickness of the oxide layer[m], which is set by the experimental data in the current work.  $\lambda$  is an empirical multiplication factor taking into account the stacking between the hydride platelet and the fraction of radial orientation due to the Zr-2 texture. Detailed studies on the hydride distribution and orientation in combination with a micromechanical models<sup>26</sup>) would be required to compute the effective hydride rim depth, a constant  $\lambda = 12$  is set for the current work.

### 3 Fracture Strain

Neglect the radial strain, a fracture plastic strain at plane strain condition assuming isotropic plasticity is given as<sup>27</sup>):

$$\varepsilon^p = \left( \frac{\sigma_0}{k} \right)^{1/n} \left\{ \frac{k^{1/n}}{\sigma_0^{1/n-1} E} \left( \frac{K_c^2}{K_e^2} - 1 \right) \right\}^{1/(1-n)} \quad (15)$$

where  $k$  is the strength coefficient.

$\sigma_0$  is the yield stress.

$n$  is the strain-hardening exponent.

$K_c$  is the fracture toughness.

$E$  is the elastic modulus.

$K_e$  is the stress intensity factor.

For a single crack

$$K_e = F \sigma \sqrt{\pi a_e} \quad (16)$$

From the Equation<sup>16</sup>)

$$F = 1.12 - 0.231 \left( \frac{a}{W} \right) + 10.55 \left( \frac{a}{W} \right)^2 - 21.72 \left( \frac{a}{W} \right)^3 + 30.39 \left( \frac{a}{W} \right)^4 \quad (17)$$

$W$  is the thickness of the cladding.  $a$  is the initial depth of crack from Eq. (14).  $a_e$  is the crack depth with plastic zone correction:

$$a_e = a + \frac{1}{2\pi} \left( \frac{K_e}{\sigma_0} \right)^2 \quad (18)$$

Using the material property from MATPRO in FRAPTRAN, the fracture strain in Eq. (15) is calculated at each time step and compared with the cladding plastic hoop strain. Once the deformation is larger than the fracture strain, PCMI failure occurs.

## 4 Results

The results of application of the PCMI model are shown in Table 2. As can be seen, the failure by PCMI could be predicted, but the enthalpy at failure is lower than the measurement data. This could be due primarily to the idealized assumption for crack propagation which neglects the enthalpy required for the propagation of crack in the ductile substrate and the Zr liner of the cladding. This indicates that the enthalpy at failure is somehow controlled by the crack propagation in the remaining ductile ligament. To demonstrate the effects of power pulse on PCMI failure, the power pulse for the case FK9 is artificially modified. The width of the modified power pulse is made ten times the original one, comparable to the power pulse at LWR conditions. The magnitude is one tenth of the original one to achieve similar enthalpy deposit. It can be seen from Table 3 that at an enthalpy of 91.1 cal/g, no failure is predicted for the wider power pulse case. The fracture strain is found to be larger than the original case with narrow power pulse. For the wider pulse case, some amount of heat transferred out to the coolant and the temperature redistribution in the pellet during the power pulse may mitigate the loading force. The stress intensity as a function of hoop stress would decrease. As a result, the fracture strain increased. Therefore the enthalpy deposition rate could play two roles in the PCMI failure: i) The enthalpy required for the onset of crack propagation ii) The enthalpy required for the crack propagation in the ductile ligament. The former could be sensitive to the loading pattern. For a wider power pulse, a higher threshold of the enthalpy is required for PCMI failure.

## IV Conclusions

The FK test series have been simulated and compared to the prediction of the FGR and PCMI models assembled in the FRAPTRAN code. Preliminary investigation shows general good agreement with the experimental data of fission gas release and mechanical response in these test cases.

Application of the FGR model reveals that the relatively larger gap sizes in the BWR fuel rods at cold zero power (CZP) conditions would enable fission gas release in the early phase of the transient. This reduces cladding deformation.

Application of the PCMI model based on fracture mechanics to the BWR fuel rods found that the model is capable of partitioning the failed and non-failed cases capturing the effects of different burnup levels and fuel enthalpy deposition. Furthermore, the model indicates that the enthalpy deposition at failure is somehow controlled by the crack propagation in the remaining ductile ligament. This model also reveals for a wider power pulse, a higher threshold of the enthalpy is required for PCMI failure.

## Acknowledgments

This work has been partially supported by the Nuclear Regulatory Commission.

## References

- 1) T. Fuketa, et al., "NSRR/RIA Experiments with High-burnup PWR Fuels," *Nuclear Safety*, 37[4], 328 (1996).
- 2) J. Papin, et al., "French Studies on High Burnup Fuel Transient Behavior under RIA Conditions," *Nuclear Safety* 37[4], 289 (1996).
- 3) V. Asmolov and L. Yegorova, "Investigation of the Behavior of VVER Fuel under RIA Conditions," *International Topical Meeting on LWR Fuel Performance*, Portland, U. S., March 2-6, (1997).
- 4) D. Sunderland, R. Montgomery and O. Ozer "Evaluation of Recent RIA-Simulation Experiments with the FALCON Fuel Performance Code," *Proceedings of the 2004 International Meeting on*

- LWR Fuel Performance*, Orlando, U. S., Sep 19-22, (2004).
- 5) W. Liu, A. Romano and M. S. Kazimi, "Modeling High-Burnup LWR Fuel Fission Gas Released and Swelling During Fast Transients," *Proceedings of the 2004 International Meeting on LWR Fuel Performance*, Orlando, U. S., Sep 19-22, (2004).
  - 6) T. Nakamura, M. Yoshinaga et al., "Boiling Water Reactor Fuel Behavior under Reactivity Initiated Accident Conditions at Burnup of 41 to 45 Gwd/tonne U", *Nuclear Technology*, 129[2], 141 (2000).
  - 7) T. Nakamura, K. Kusagaya, T. Fuketa and H. Uetsuka, "High-burnup BWR Fuel Behavior under Simulated Reactivity Initiated Accident Conditions," *Nuclear Technology*, 138[3], 246 (2002).
  - 8) T. Nakamura, et al., "Evaluation of Burnup Characteristics and Energy Deposition During NSRR Pulse Irradiation Tests on Irradiated BWR Fuels," JAERI-Research 2000-048, Japan Atomic Energy Research Institute (2000) [In Japanese].
  - 9) T. Nakamura, et al., "High Burnup (41-61GWd/tU) BWR Fuel Behavior under Reactivity Initiated Accident Conditions," JAERI-Research 2001-054, Japan Atomic Energy Research Institute (2001) [In Japanese].
  - 10) K. Lassmann, C. T. Walker, J. van de Laar and F. Lindström, "Modelling the high burnup UO<sub>2</sub> structure in LWR fuel," *Journal of Nuclear Materials*, 226[1-2], 1 (1995).
  - 11) K. J. Geelhood, C. E. Beyer and M. E. Cunningham, "Modifications to FRAPTRAN to Predict Fuel Rod Failures Due to PCMI During RIA-type Accidents," *Proceedings of the 2004 International Meeting on LWR Fuel Performance*, Orlando, U. S., Sep 19-22, (2004).
  - 12) F. Lemoine, J. Papin, J. Frizonnet, B. Cazalis and H. Rigat, "The Role of Grain Boundary Fission Gases in High Burnup Fuel under Reactivity Initiated Accident Conditions," *Proc. of the Fission Gas Behaviour in Water Reactor Fuels Seminar*, OECD, Cadarache, France, Sep 26-29, (2000)
  - 13) J. Spino, D. Baron, M. Coquerelle and A. D. Stalios, "High Burn-up Rim Structure: Evidences that Xenon-depletion, Pore Formation and Grain Subdivision Start at Different Local Burn-ups," *Journal of Nuclear Materials*, 256[2-3], 189 (1998).
  - 14) L. C. Bernard, J. L. Jacoud and P. Vesco, "An Efficient Model for the Analysis of Fission Gas Release," *Journal of Nuclear Materials* 302[2], 125 (2002).
  - 15) T. Nakamura, T. Fuketa, T. Suigiyama and H. Sasajima, "Failure Thresholds of High Burnup BWR Fuel Rods under RIA Conditions," *Journal of Nuclear Science and Technology*, 37[1], 37 (2004).
  - 16) M. Kuroda, S. Yamanaka, F. Nagase and H. Uetsuka, "Analysis of the Fracture Behavior of Hydrided Fuel Cladding by Fracture Mechanics," *Nuclear Engineering and Design*, 203[2], 185 (2001).
  - 17) F. Nagase and T. Fuketa, "Investigation of Hydride Rim Effect on Failure of Zircaloy-4 Cladding with Tube Burst Test," *Journal of Nuclear Science and Technology*, 42[1], 58 (2005).
  - 18) K. Edsinger, et al., "Degraded Fuel Cladding Fractography and Fracture Behavior," *Zirconium in the Nuclear Industry: 12th International Symposium*, ASTM STP 1354, American Society for Testing and Materials, 316 (2000).
  - 19) V. Grigoriev, B. Josefsson, and B. Rosberg, "Fracture Toughness of Cladding Tubes," *Zirconium in the Nuclear Industry: 11th International Symposium*, ASTM STP 1295, American Society for Testing and Materials, 431 (1996).

- 20) P. H. Kreyens et al., "Embrittlement of Reactor Core Materials," *Zirconium in the Nuclear Industry: 11th International Symposium*, ASTM STP 1295, American Society for Testing and Materials, 758 (1996).
- 21) S. B. Wisner and R. B. Adamson, "Combined Effects of Radiation Damage and Hydrides on the Ductility of Zircaloy-2," *Nuclear Engineering and Design*, 185[1], 33 (1998).
- 22) A. M. Garde, "Influence of Cladding Microstructure on the Low Enthalpy Failures in RIA Simulation Tests," *Zirconium in the Nuclear Industry: 12th International Symposium*, ASTM STP 1354, American Society for Testing and Materials, 234 (2000).
- 23) G. Domizzi, R. A. Enrique, J. Ovejero-García and G. C. Buscagliaet, "Blister Growth in Zirconium Alloys: Experimentation and Modeling," *Journal of Nuclear Materials* 229[2], 36 (1996).
- 24) A. Sawatzky, "The Diffusion and Solubility of Hydrogen in the Alpha-Phase of Zircaloy," *Journal of Nuclear Materials* 2[1], 62(1960)
- 25) A. Sawatzky and B. J. S. Wilkins, "Hydrogen Solubility in Zirconium Alloys Determined by Thermal Diffusion," *Journal of Nuclear Materials* 22[3], 304 (1967)
- 26) K. S. Chan, "Micromechanical Model for Predicting Hydride Embrittlement in Nuclear Fuel Cladding Material," *Journal of Nuclear Materials*, 227[3], 200 (1996).
- 27) O. N. Pierron, D. A. Koss, A. T. Motta and K. S. Chan, "The Influence of Hydride Blisters on the Fracture of Zircaloy-4," *Journal of Nuclear Materials*, 322[1], 21 (2003).

Table 1 Test Conditions for FK1-FK9

	FK1	FK2	FK3	FK4	FK5	FK6	FK7	FK8	FK9
Local burnup (GWd/tU)	45	45	41	56	56	61	61	61	61
Maximum oxide thickness (micron)	21.5	24	25.8	15	15	27	27	27	27
Maximum hydrogen concentration (ppm)	72	72	72	82	82	220	220	159	159
Peak linear heat rate (W/cm)	228	228	209	350	350	350	350	350	350
Peak fuel enthalpy (J/g)	130	70	145	140	70	130	129	65	90
Pulse width (ms)	4.5	7	4.5	4.3	7.3	4.3	4.3	7.3	5.7
Maximum cladding residual hoop strain (%)	0.85	0	1.5	1.25	0	<0.1	<0.1	<0.02	-
Fission gas release (%)	8.2	3.1	4.7	15.7	9.6	16.9	17	11.3	16.6
[base irradiation]	1.5	1.5	0.35	12.5	12.5	14.2	14.2	12	12

Table 2 PCMI failure Prediction\*

	<i>a</i> ( $\mu\text{m}$ )	Failure	Failure Enthalpy (cal/g)	Failure time (sec)
FK1	43.8	No /No	-	-
FK2	46.3	No /No	-	-
FK3	48.1	No /No	-	-
FK4	43.2	No /No	-	-
FK5	43.2	No /No	-	-
FK6	137.8	Yes /Yes	70 /42.3	0.2440 /0.2431
FK7	137.8	Yes /Yes	62 /54.6	0.2443 /0.2436
FK8	137.8	No /No	-	-
FK9	137.8	Yes /Yes	86 /67.3	0.2692 /0.2651

\*Measurement/Prediction

Table 3 Power pulse effect on PCMI failure

	Original power pulse	Modified power pulse
Pulse width (ms)	5.7	57
Fracture strain (%)	0.47 <sup>a</sup>	0.84 <sup>b</sup>
Peak P/C interface pressure (MPa)	68.9 <sup>a</sup>	62.9
Fuel enthalpy (cal/g)	67.3 <sup>a</sup>	91.1

<sup>a</sup> Value at failure time<sup>b</sup> Minimum value during PCMI loading

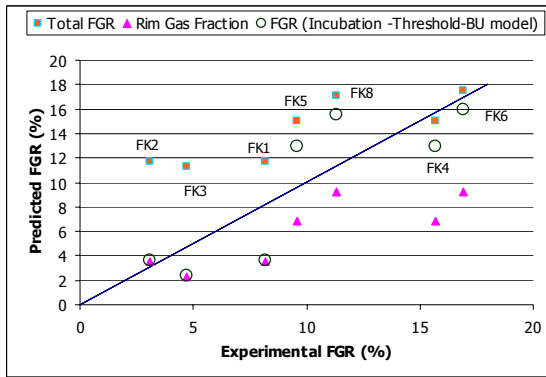


Figure 1 Comparison of FGR predicted by code calculation and measured in experiments

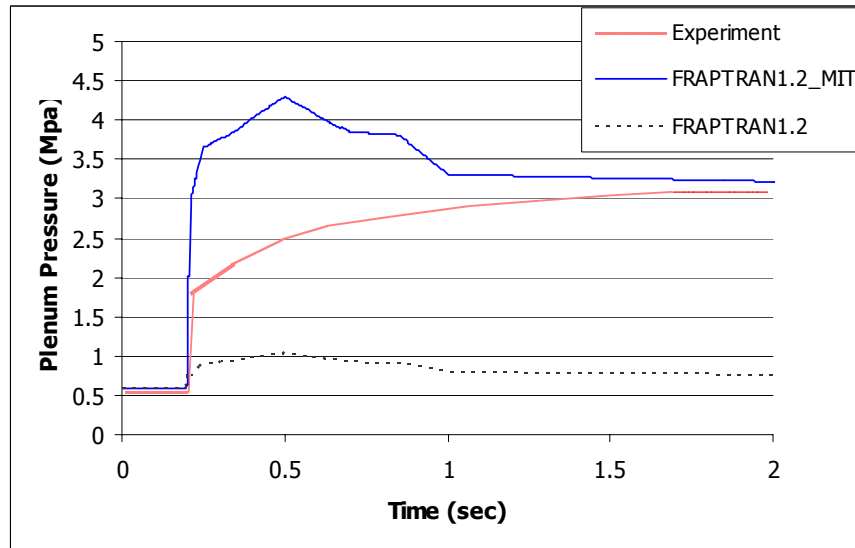


Figure 2 Comparison of Plenum pressure predicted by FRAPTRAN and measured in experiment for FK4

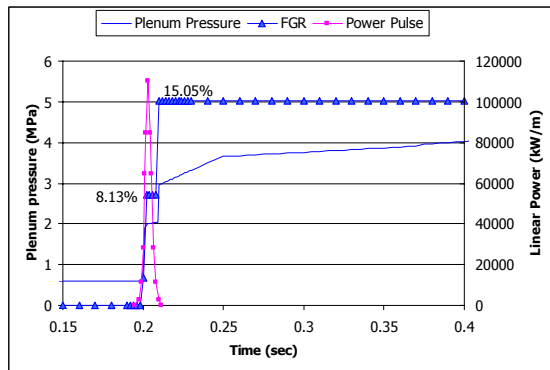


Figure 3 FGR kinetics for FK4 calculated by FRAPTRAN1.2\_MIT

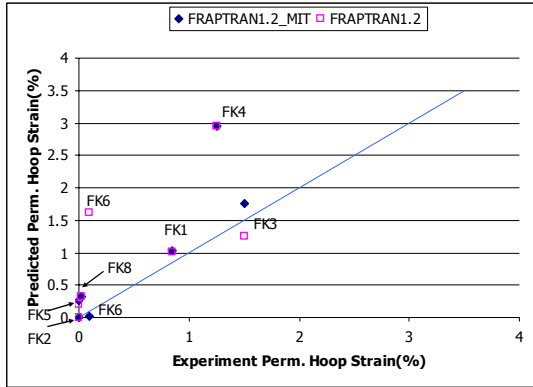


Figure 4 Comparison of permanent hoop strain predicted by FRAPTRAN with experiments

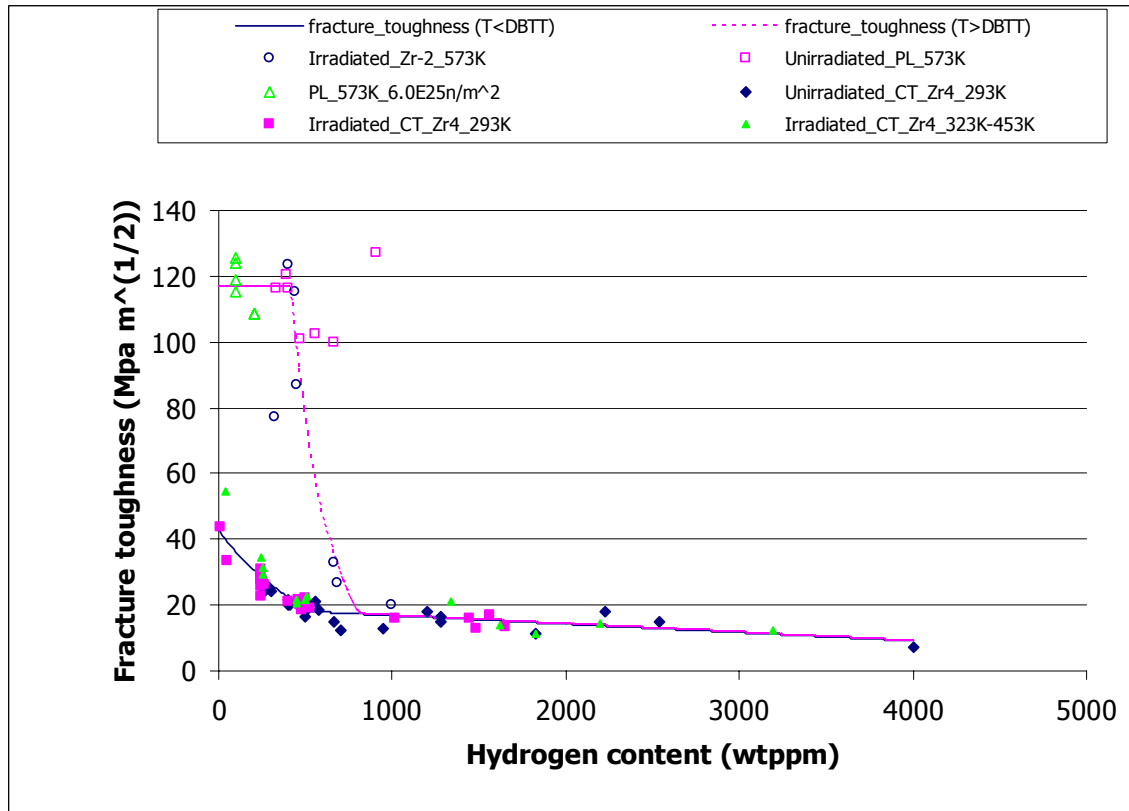


Figure 5 Fracture toughness versus hydrogen content